

## Original Article

**Cite this article:** Liu Y, Liu X, Ma L, Kang S, Qiang X, Guo F, and Sun Y (2020) Temporal–spatial variations in aeolian flux on the Chinese Loess Plateau during the last 150 ka. *Geological Magazine* **157**: 757–767. <https://doi.org/10.1017/S0016756819001067>

Received: 30 January 2019

Revised: 30 June 2019

Accepted: 5 August 2019

First published online: 14 November 2019


**Keywords:**

Chinese Loess Plateau; aeolian flux; temporal–spatial variations; glacial–interglacial cycle

**Author for correspondence:**

Youbin Sun, Email: [sunyb@ieecas.cn](mailto:sunyb@ieecas.cn)

# Temporal–spatial variations in aeolian flux on the Chinese Loess Plateau during the last 150 ka

Yuming Liu<sup>1,2</sup> , Xingxing Liu<sup>1,3</sup>, Long Ma<sup>4</sup>, Shugang Kang<sup>1,3</sup>, Xiaoke Qiang<sup>1,3</sup>, Fei Guo<sup>1,2</sup> and Youbin Sun<sup>1,3</sup>

<sup>1</sup>State Key Laboratory of Loess and Quaternary Geology, Institute of Earth Environment, Chinese Academy of Sciences, Xi'an 710061, China; <sup>2</sup>College of Earth and Planetary Sciences, University of Chinese Academy of Sciences, Beijing 100049, China; <sup>3</sup>CAS Centre for Excellence in Quaternary Science and Global Change, Chinese Academy of Sciences, Xi'an 710061, China and <sup>4</sup>State Key Laboratory of Continental Dynamics and Shaanxi Key Laboratory of Early Life and Environment, Department of Geology, Northwest University, Xi'an 710069, China

**Abstract**

Aeolian dust deposits from continent and ocean have been extensively investigated to reflect past changes in source aridity and atmospheric circulations. Aeolian flux (AF) as a quantitative dust proxy has been widely used in both palaeoenvironmental reconstruction and numerical simulation. However, available AF data on the Chinese Loess Plateau (CLP) is too limited to assess the temporal–spatial variations at glacial–interglacial timescales, and therefore cannot be used as robust input parameters in palaeoclimate models. Here we investigate eight loess profiles along two N–S-aligned transects on the CLP to quantitatively estimate the AF variations over the last glacial–interglacial cycle. We first establish a refined chronological framework based on optically stimulated luminescence chronology and pedostratigraphic correlation. AF was then estimated by multiplying the sedimentation rate and bulk density. The results show that the AF increases from 2–18 g cm<sup>-2</sup> ka<sup>-1</sup> in the southeastern CLP to 14–105 g cm<sup>-2</sup> ka<sup>-1</sup> in the northwestern CLP. At glacial–interglacial scales, the AF varies from 2–20 g cm<sup>-2</sup> ka<sup>-1</sup> during the last interglacial to 8–105 g cm<sup>-2</sup> ka<sup>-1</sup> in the last glaciation. Due to more spatial coverage and better age constraints, our AF data can be used to refine other AF datasets and to improve the proxy–model comparison.

**1. Introduction**

In recent decades, aeolian dust deposits have been widely investigated from Chinese loess–red clay sequences (e.g. An *et al.* 1991a, 2001; Kohfeld & Harrison, 2003; Sun & An, 2005; Kang *et al.* 2013, 2015), Pacific pelagic sediments (e.g. Pye & Zhou, 1989; Rea, 1994; Rea *et al.* 1998; Winckler *et al.* 2008; Zhang *et al.* 2016, 2018b; Jacobel *et al.* 2017) and Greenland ice cores (e.g. Yung *et al.* 1996; EPICA Community Members, 2004) to reflect changes in the Asian dust cycle and the monsoon–arid environmental system. As a quantitative proxy of the dust input, aeolian flux (AF) has been employed to infer the drying history in Asian inland (e.g. An *et al.* 1991a; Rea *et al.* 1998; Kohfeld & Harrison, 2001, 2003; Sun & An, 2005; Kang *et al.* 2015; Zhang *et al.* 2016) and to improve the understanding of Asian dust cycling from regional to hemispheric scales (Pye & Zhou, 1989; Kohfeld & Harrison, 2001, 2003; Nilson & Lehmkuhl, 2001; Shi & Liu, 2011; Muhs, 2013).

Previous AF reconstructions on the Chinese Loess Plateau (CLP) indicate that the Asian interior has experienced stepwise aridification and increased dry–humid fluctuations since the late Oligocene Epoch (Guo *et al.* 2002; Sun & An, 2002), linked to the growth of Tibet and global cooling (An *et al.* 2001; Zachos *et al.* 2001). At glacial–interglacial (10<sup>5</sup> years) timescales, the AFs were generally higher during glacial than interglacial periods because of the strong coupling of the source aridity and East Asian winter monsoon (EAWM) intensity with Northern Hemisphere ice-volume changes (e.g. An *et al.* 1991a; Sun & An, 2005). Spatially, Kohfeld & Harrison (2003) summarized that the AFs were relatively high in the NW CLP and decreased SE-wards over the CLP. More recently, due to the development of sensitivity-corrected optically stimulated luminescence (OSL) dating techniques for quartz, sub-orbital AF variation was detected to infer the link between the EAWM intensity and the mean position of the westerly jet (Kang *et al.* 2015).

Although previous studies have achieved the framework of AF fluctuations at tectonic and glacial–interglacial timescales (Guo *et al.* 2002; Sun & An, 2002, 2005; An *et al.* 2014), these AF data were seldom employed as input parameters to assess past dust–climate interactions in numerical simulation experiments (Harrison *et al.* 2001; Shi & Liu, 2011). One plausible reason is that available AF data are only from several classic profiles, limiting our understanding of the temporal–spatial dust flux variability. The low spatial coverage could not exclude the local outliers due to the different geomorphological setting (Kohfeld & Harrison, 2003). The other reason

is that many factors can limit AF reconstruction, including an inconsistent age model, a lack of quality bulk density and neglecting grain size data (Kohfeld & Harrison, 2003). For example, the AF uncertainty induced by different age models can be as large as 192%, and the lack of bulk density results in an AF error of  $\pm 15\%$  (Kohfeld & Harrison, 2003; Sun & An, 2005). Furthermore, grain size data is crucial for assessing different transportation processes of coarse- and fine-grained particles. In particular, particle matter with a diameter finer than  $10\ \mu\text{m}$  (PM10) is more important than the total suspended particles due to its long-range transportation (Pye & Krinsley, 1986; Prospero *et al.* 2002).

In this study, we investigate eight loess–palaeosol sequences along two N–S-aligned transects on the CLP to provide better constraints on a reconstruction of AF. We first generate a uniform age model based on OSL dating and pedostratigraphic correlation, so that chronology uncertainty can be eliminated across different profiles. The measured bulk density and grain-size data are then employed to estimate the AF of bulk samples and fine fraction. The estimated AF data can provide a robust evaluation of the temporal–spatial changes in the dust input under different interglacial–glacial boundary conditions. Finally, the PM10 AF was estimated from eight loess–palaeosol sequences, which can be used as quantitative dust input factors to improve the model capacity and evaluate the dust impact on past climate change.

## 2. Materials and methods

### 2.a. Setting and sampling

The CLP is a unique terrestrial place for aeolian dust studies due to the widespread and thick loess–palaeosol–red-clay sequences (Harrison *et al.* 2001; Kohfeld & Harrison, 2001; Derbyshire *et al.* 2003; Maher *et al.* 2010; Shao *et al.* 2011; Muhs, 2013; An *et al.* 2014). Proximal to the major Asian dust sources (Liu, 1985; Prospero, 2002; Engelbrecht & Derbyshire, 2010; Shi & Liu, 2011; An *et al.* 2014), the CLP became a predominant sink of Asian dust from 25 Ma to the present (Guo *et al.* 2002; Qiang *et al.* 2011). The EAWM and the westerlies played a key role in dust emission from the Asian inland and deposition on the CLP (Liu, 1985; An *et al.* 1991a; Porter & An, 1995; Peng *et al.* 2005; Shi & Liu, 2011). Meanwhile, the East Asian summer monsoon (EASM)-induced rainfall resulted in varying pedogenic alterations in the loess–palaeosol sequences (Kukla, 1987; An *et al.* 1991b). Furthermore, the EAWM and EASM are mainly controlled by the Northern Hemisphere ice sheets and hydroclimate on an orbital timescale (An *et al.* 2015; Sun *et al.* 2019). Chinese loess–palaeosol alternations therefore contain the imprints of changing high-latitude ice sheets and low-latitude hydroclimate (An *et al.* 2015; Sun *et al.* 2019).

Here, eight loess profiles are investigated along two N–S-aligned transects on the central CLP (Fig. 1). From north to south, the western transect consists of Guojiapan (GJP,  $37.11^\circ\text{N}$ ,  $107.39^\circ\text{E}$ , 1782 m above sea level (asl); Ma *et al.* 2017), Beiguoyuan (BGY,  $36.66^\circ\text{N}$ ,  $17.29^\circ\text{E}$ , 1506 m asl; Ma *et al.* 2017), Xifeng (XF,  $35.76^\circ\text{N}$ ,  $107.78^\circ\text{E}$ , 1250 m asl; Sun *et al.* 2006a) and Lingtai (LT,  $34.98^\circ\text{N}$ ,  $107.55^\circ\text{E}$ , 1350 m asl; Sun *et al.* 2006a), and the eastern transect contains Yanchang (YC,  $36.62^\circ\text{N}$ ,  $109.94^\circ\text{E}$ , 1107 m asl; Ma *et al.* 2017), Luochuan (LC,  $35.73^\circ\text{N}$ ,  $109.43^\circ\text{E}$ , 1094 m asl; Ma *et al.* 2017), Tongchuan (TC,  $34.97^\circ\text{N}$ ,  $108.96^\circ\text{E}$ , 797 m asl; Ma *et al.* 2017), and Bailu (BL,  $34.20^\circ\text{N}$ ,  $109.19^\circ\text{E}$ , 730 m asl;

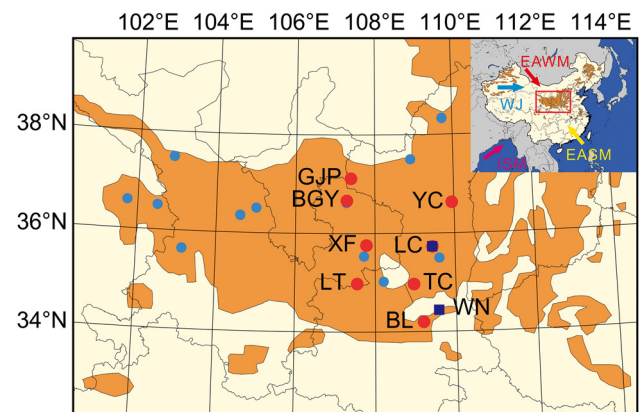


**Fig. 1.** Location map. Orange areas show the distribution of Chinese loess; the largest area in the middle region is the Chinese Loess Plateau. Red dots indicate the eight profiles in this study. Light blue dots indicate the profiles with OSL dates. Dark blue squares represents the profiles Luochuan (LC; Lu *et al.* 2007) and Weinan (WN; Kang *et al.* 2011, 2013) with high-resolution OSL ages, which were used to establish chronologies. ISM – Indian summer monsoon; EASM – East Asian summer monsoon; EAWM – East Asian winter monsoon; WJ – westerly jet.

Ma *et al.* 2017). As established by Kukla (1987), the loess and palaeosol units are referred to as  $L_i$  and  $S_j$ , where  $i$  is the index from top to bottom. A postfix  $LL_j/SS_j$  will be appended to  $L_i/S_i$  to denote the sublayer, where  $j$  is the index of current loess/palaeosol layer. All profiles contain the upper part of the penultimate glaciation ( $L_2$ ), last interglacial loess ( $S_1$ ), last glacial loess ( $L_1$ ) and the Holocene loess ( $S_0$ ), except for the Yanchang section that does not have the  $S_0$  unit. Within the  $L_1$  unit, one moderately weathered palaeosol layer ( $L_1SS_1$ ) has developed; in some profiles (e.g. Weinan (WN) and Xifeng)  $L_1SS_1$  can be defined as two palaeosol layers intercalated by a thin loess layer (Kukla & An, 1989; Guo *et al.* 1996). Based on previous studies (Ding *et al.* 2002),  $S_0$ ,  $L_1LL_1$ ,  $L_1SS_1$ ,  $L_1LL_2$  and  $S_1$  can be roughly correlated with marine isotope stages (MIS) 1–5. The thickness of these profiles decreases from 44.6 m at Guojiapan to 9.5 m at Bailu, mainly due to the varying sedimentation rate of the last glacial loess. Powder samples of Lingtai and Xifeng at 10 cm interval were obtained from previous work (Sun *et al.* 2006a). In this study, we collected powder samples at 2 cm intervals from Guojiapan, Beiguoyuan and Bailu, at 5 cm intervals from Yanchang and Tongchuan, and at 10 cm intervals from Luochuan.

### 2.b. Measurements of magnetic susceptibility, grain size and bulk density

Magnetic susceptibility (MS) of dry powder samples was measured using a Bartington MS2 meter. The grain size of bulk samples was determined using a Malvern 2000 laser instrument, after removal of the organic matter and carbonate (Lu & An, 1997). Bulk density was estimated by the oil-soaked method (Sun *et al.* 2000). All the powder samples were involved in the measurements of MS and grain size, but the bulk density data are relatively sparse at c. 15–20 cm intervals. All these measurements were conducted at the Institute of Earth Environment, Chinese Academy of Sciences. Note that MS ( $10^{-8}\ \text{m}^3\ \text{kg}^{-1}$ ), mean grain size (MGS,  $\mu\text{m}$ ) and AF ( $\text{g cm}^{-2}\ \text{ka}^{-1}$ ) data for Xifeng and Lingtai were published by Sun & An (2005), and MS ( $10^{-8}\ \text{m}^3\ \text{kg}^{-1}$ ) and MGS ( $\mu\text{m}$ ) for Guojiapan, Beiguoyuan, Yanchang, Tongchuan and Bailu during the last interglacial were published by Ma *et al.* (2017).

### 2.c. Chronology and AF calculation

The OSL dating can generate a high-resolution age model for several classic loess profiles such as Luochuan (Lu *et al.* 2007), Yuanbao (Lai *et al.* 2007; Rao *et al.* 2013), Jingyuan (Sun *et al.* 2010) and Gulang (Sun *et al.* 2012). Although some studies have detected the depositional hiatus at the edge of the CLP (e.g. Lu *et al.* 2006; Stevens *et al.* 2018; Wu *et al.* 2019), the continuity of its main body is widely approved (Lu *et al.* 2007; Lai *et al.* 2007; Sun *et al.* 2010, 2012; Rao *et al.* 2013; Zhang *et al.* 2018a). Many high-resolution OSL studies have proven that an age model based on pedostratigraphy, magnetic susceptibility or grain size could be significantly different from the independent OSL-based age model (Stevens *et al.* 2006, 2007, 2008, 2018; Lai & Wintle, 2006; Lu *et al.* 2006; Sun *et al.* 2010; Xu *et al.* 2018). A uniform basis of division, magnetic susceptibility and/or mean grain size, was applied to these profiles to ensure the synchronicity of boundaries. In order to establish the chronology of the profiles that have no independent ages, there are three criteria for selecting the independent OSL profiles by correlation of MS and/or MGS, respectively. First and foremost, the record length had to span the last interglacial and be free of documented sedimentary hiatuses. Second, the records had to be independently dated. Third, the profiles must have magnetic susceptibility and/or mean grain size records. Closely spaced OSL dates of the Weinan profile offer a robust chronology spanning the last 130 ka (Kang *et al.* 2011, 2013, 2015), consistent of the OSL chronology of the classic Luochuan profile (Lu *et al.* 2007). Here we combine the OSL dates and proxy variations of these two profiles to generate uniform time controls for five key pedostratigraphic boundaries (e.g.  $L_2/S_1$ ,  $S_1/L_1$ ,  $L_1LL_2/L_1SS_1$ ,  $L_1SS_1/L_1LL_1$ ,  $L_1/S_0$ ).

Considering that the colour of loess-palaeosol may vary little in some profiles, the boundaries were identified mainly by the remarkable changes in MGS; MS records were considered as supplementary. Because the signals of MGS are not as vulnerable as that of MS to the influence of post-depositional processes (Sun *et al.* 2006a, b; 2010; Dong *et al.* 2015). The ages of these boundaries were determined by these two OSL age models (Fig. 2). At the Weinan profile, the ages of five boundaries were estimated to be 11.8, 30.1, 64.1, 79.3 and 127.0 ka (Fig. 2d–f). The ages of five boundaries at Luochuan were estimated to be 8.6, 29.5, 57.8, 73.5 and 126.5 ka (Fig. 2g, h). Due to the OSL dating errors, we adopted the average ages of these five boundaries (i.e. 10.2, 29.8, 61.0, 76.4 and 126.8 ka) as the time controls for the chronological reconstruction (Fig. 3). The weighted grain-size age model that assumes that the sedimentation rate is related to the grain size was applied to refine the chronologies (Porter & An, 1995). This approach can generate a comparable chronology and a good match between proxy variations for all profiles.

The AF ( $g\ cm^{-2}\ ka^{-1}$ ) is estimated by multiplying sedimentation rate by bulk density. The sedimentation rate ( $cm\ ka^{-1}$ ) is calculated as thickness/duration, which is dependent on the chronology. The bulk density was linearly interpolated due to its relatively low resolution. Meanwhile, PM10 AF was estimated as  $AF_{PM10} = P_{PM10} \times AF$ , where  $P_{PM10}$  is the proportion of PM10 derived from the grain size distribution data.

## 3. Results

### 3.a. Variations in magnetic susceptibility, grain size, bulk density and sedimentation rate

The magnetic susceptibility and grain size of Chinese loess are typical proxies of variations in the EASM and EAWM intensities

(An *et al.* 1990, 1991a,b). Consistent with previous studies, the  $S_0$  and  $S_1$  units are characterized by higher MS and finer MGS, while the  $L_1$  layers have lower MS and coarser MGS (Fig. 3). The MS values of the eight profiles vary over the range  $27.9\text{--}290.5 \times 10^{-8}\ m^3\ kg^{-1}$ . The highest MS appears in the  $S_1$  unit of Bailu; meanwhile, the  $L_1LL_1$  layer of Guojiapan holds the lowest value of MS (Fig. 3). As shown in Table 1, the loess-palaeosol layers from high MS average to low MS average are  $S_1$  ( $72.0\text{--}250.6 \times 10^{-8}\ m^3\ kg^{-1}$ ),  $S_0$  ( $95.6\text{--}232.9 \times 10^{-8}\ m^3\ kg^{-1}$ ),  $L_1SS_1$  ( $38.6\text{--}204.4 \times 10^{-8}\ m^3\ kg^{-1}$ ),  $L_1LL_1$  ( $35.6\text{--}146.7 \times 10^{-8}\ m^3\ kg^{-1}$ ) and  $L_1LL_2$  ( $34.4\text{--}180.1 \times 10^{-8}\ m^3\ kg^{-1}$ ). Spatially, the MS values from SE profiles (e.g.  $107.0\text{--}290.5 \times 10^{-8}\ m^3\ kg^{-1}$  at Bailu) are generally higher than that of NW profiles (e.g.  $27.9\text{--}116.0 \times 10^{-8}\ m^3\ kg^{-1}$  at Guojiapan). Furthermore, for the east transect the MS ratios of MIS 2/5 decrease from south (e.g. 0.60 at Bailu) to north (e.g. 0.23 at Yanchang), while for the west transect, the ratios increase from the middle (e.g. 0.34 at Xifeng) to the end (e.g. 0.50 at Guojiapan and 0.64 at Lingtai). In addition, the MS records at Guojiapan and Beiguoyuan (located in the NW CLP) clearly exhibit three peaks in  $S_1$  and correlate well with the three weak sub-palaeosol layers ( $S_1SS_1$ ,  $S_1SS_2$  and  $S_1SS_3$ ) (Fig. 3).

The MGS of the eight profiles varies from 12.20 to  $61.16\ \mu m$  since last interglacial. Similar to MS, the minimum and maximum values of MGS appear in the  $S_1$  of Bailu and the  $L_1LL_1$  of Guojiapan, respectively. The stage averages of MGS (Table 1) from low to high are obtained from  $S_1$  ( $11.46\text{--}25.36\ \mu m$ ),  $L_1SS_1$  ( $14.35\text{--}31.96\ \mu m$ ),  $S_0$  ( $16.02\text{--}34.73\ \mu m$ ),  $L_1LL_2$  ( $14.64\text{--}38.38\ \mu m$ ) and  $L_1LL_1$  ( $17.09\text{--}45.92\ \mu m$ ), respectively. For each stage, the MGS records all display a significantly south–north spatial increase; however, the MGS ratios of MIS 2/5 display a consistent south–north increase in both transects. In addition,  $P_{PM10}$  (Fig. 3, purple curves), as for MGS, has a high negative correlation with MS.

Similar to the MS and MGS variations, the values of bulk density exhibit significantly glacial–interglacial fluctuations (Fig. 3, green curves) in Xifeng, Lingtai, Yanchang, Luochuan and Tongchuan profiles, while this fluctuation is not evident in Guojiapan and Beiguoyuan profiles. In general, bulk density values are relatively low in glacial  $L_1LL_1$  ( $1.14\text{--}1.82\ g\ cm^{-3}$ ) compared with that in interglacial  $S_1$  ( $1.42\text{--}1.87\ g\ cm^{-3}$ ). Spatially, the bulk density values exhibit a southwards decrease from Guojiapan ( $1.18\text{--}1.54\ g\ cm^{-3}$ ) to Beiguoyuan ( $1.29\text{--}1.49\ g\ cm^{-3}$ ), Xifeng ( $1.51\text{--}1.90\ g\ cm^{-3}$ ) and Lingtai ( $1.53\text{--}2.0\ g\ cm^{-3}$ ), and from Yanchang ( $1.14\text{--}1.66\ g\ cm^{-3}$ ) to Luochuan ( $1.28\text{--}1.59\ g\ cm^{-3}$ ), Tongchuan ( $1.27\text{--}1.71\ g\ cm^{-3}$ ) and Bailu ( $1.26\text{--}1.87\ g\ cm^{-3}$ ). The average value of bulk density is about  $1.4 \pm 0.1\ g\ cm^{-3}$  in most profiles (i.e. Guojiapan, Beiguoyuan, Yanchang, Luochuan and Tongchuan), which is lower than that for Xifeng ( $1.65\ g\ cm^{-3}$ ), Lingtai ( $1.76\ g\ cm^{-3}$ ) and Bailu ( $1.51\ g\ cm^{-3}$ ). The bulk density ranges between loess and palaeosol layers are larger in the profiles from northern and southern CLP ( $0.4\text{--}0.6\ g\ cm^{-3}$ ) than those in the central CLP ( $0.2\text{--}0.3\ g\ cm^{-3}$ ).

The sedimentation rate records (Fig. 3, orange curves) also show obvious orbital variability from the NW CLP to the SE CLP. For example, at the Guojiapan profile (Fig. 3a, orange curve), the averages of MIS 1–5 are 25.4, 55.1, 39.6, 49.6 and  $14.5\ cm\ ka^{-1}$ . In other words, the sedimentation rate records are generally higher during the glacial/stadial periods. Furthermore, the sedimentation rate records in the NW CLP (e.g.  $10.25\text{--}75.58\ cm\ ka^{-1}$  at Guojiapan profile) are much higher than these in the SE CLP (e.g.  $1.25\text{--}11.21\ cm\ ka^{-1}$  at Bailu profile).



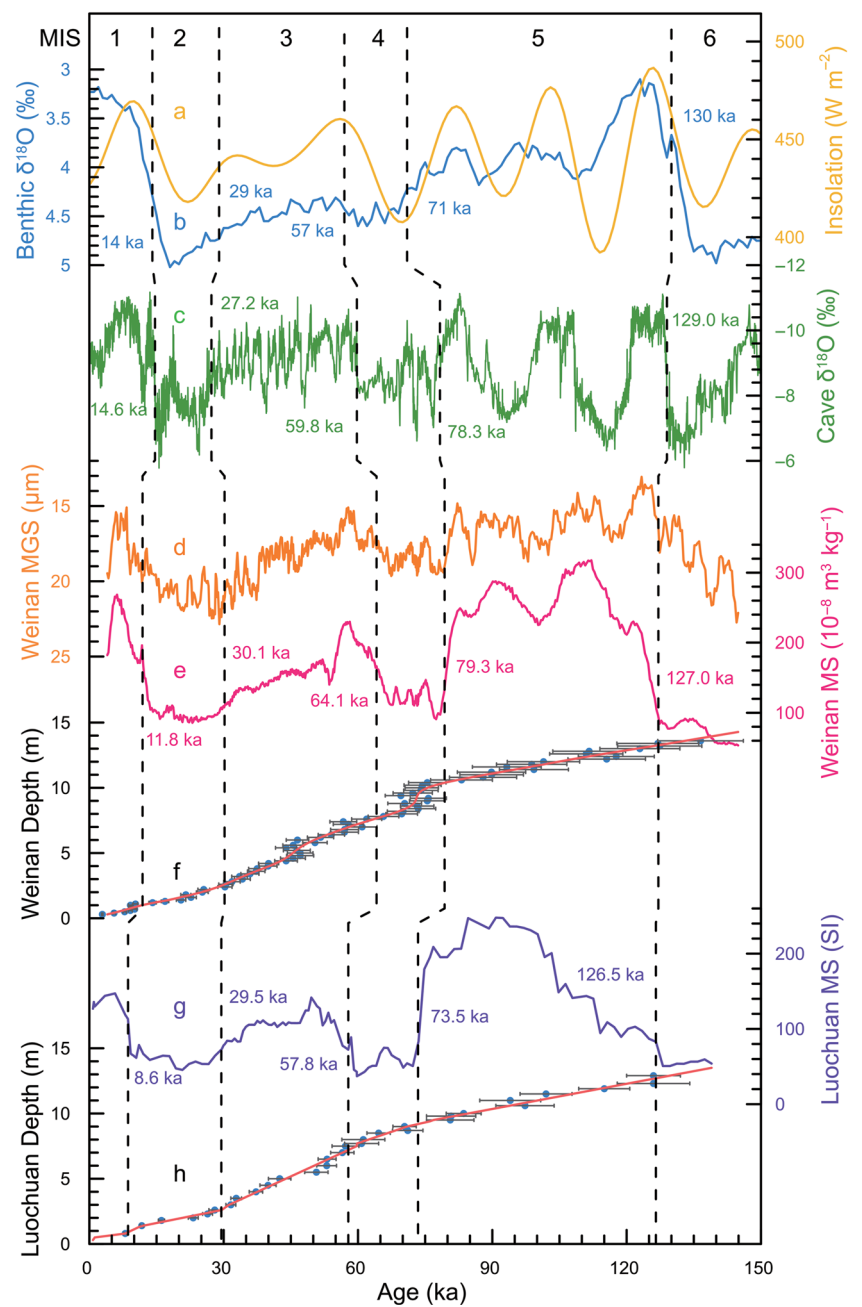


**Fig. 2.** Comparison of different chronologies: a, July insolation at 65° N (yellow; Berger, 1978); b, benthic  $\delta^{18}\text{O}$  (blue; Lisiecki & Raymo, 2005); c, Chinese cave  $\delta^{18}\text{O}$  (green; Cheng *et al.* 2016); d, Weinan mean grain size (MGS; orange; Kang *et al.* 2011, 2013); e, Weinan magnetic susceptibility (MS; pink; Kang *et al.* 2011, 2013); f, Weinan age–depth model (Kang *et al.* 2011, 2013); g, Luochuan magnetic susceptibility (MS; purple; Lu *et al.* 2007); and h, Luochuan age–depth model (Lu *et al.* 2007) since the last interglacial. In f and h, blue dots with black bars are OSL dates and red curves are the fitting age model. Black dashed lines show the boundaries of marine isotope stages (MIS).

### 3.b. AF and $AF_{PM10}$ fluctuations

In general, AF and  $AF_{PM10}$  exhibit similar glacial–interglacial fluctuations (Fig. 4, orange and purple curves). These two flux records are higher and more variable in the last glacial than those in the last interglacial and Holocene.  $S_1$  is characterized by the lowest fluxes ( $2\text{--}40\text{ g cm}^{-2}\text{ ka}^{-1}$ ) over the entire CLP, compared with the fluxes of other stratigraphic layers. As an interstadial of last glacial, MIS 3 generally has lower AFs compared with those of MIS 2 and MIS 4 (Table 1). Unlike MS and MGS, the AF ratio for MIS 2/5 is not regular enough. There is a distinct decrease in AF from NW to SE during each stage (Table 1). For example, the average AF at Guojiajan during MIS 2 reaches  $75.89\text{ g cm}^{-2}\text{ ka}^{-1}$ , whereas the value is  $11.15\text{ g cm}^{-2}\text{ ka}^{-1}$  at Bailu. Notably, the averages of Lingtai during MIS 2 and MIS 5 are higher than that of Xifeng, although Xifeng is to the north of Lingtai.  $AF_{PM10}$  is generally similar to AF, but has a small

range. AF records vary from  $2$  to  $110\text{ g cm}^{-2}\text{ ka}^{-1}$ , whereas the range of  $AF_{PM10}$  is  $0.8\text{--}15.6\text{ g cm}^{-2}\text{ ka}^{-1}$ .

## 4. Discussion

### 4.a. Glacial–interglacial AF fluctuations linked to ice-volume change

The averages of AF during MIS 1–5 were calculated (Table 1). Because the ages of MIS 1 are extrapolated by its overall sedimentation rate, the AFs of MIS 1 may be biased. Nevertheless, the result shows that the AFs are highest during MIS 2 or MIS 4 and are lowest during MIS 5. The average AFs during MIS 1–5 are  $27.9$ ,  $47.9$ ,  $21.1$ ,  $42.3$  and  $10.6\text{ g cm}^{-2}\text{ ka}^{-1}$  (Kohfeld & Harrison, 2003), comparable with the results of this study (Table 1, Fig. 5). It should be noted that the averages of MIS 2 and MIS 4 estimated by Kohfeld &

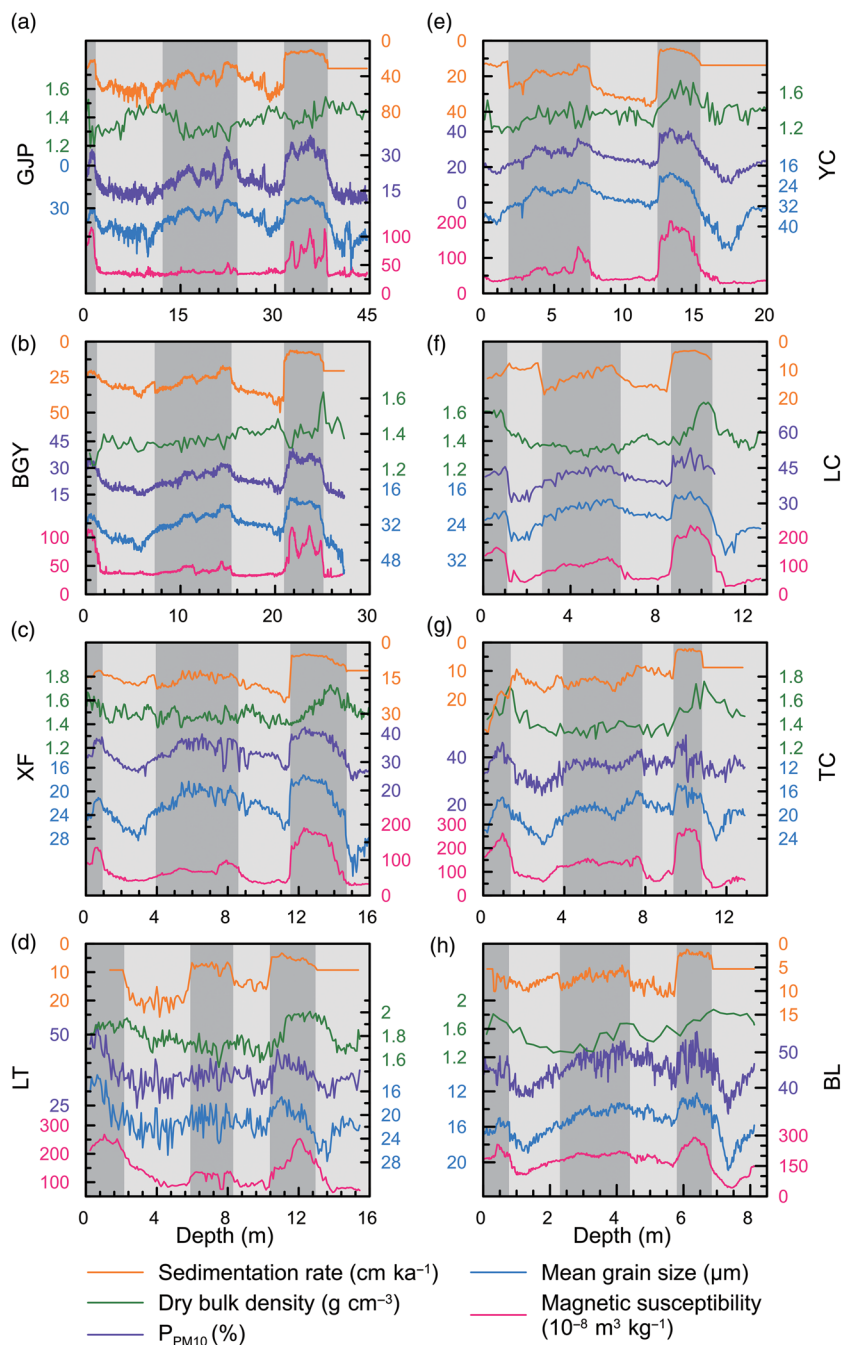


**Fig. 3.** The proxies and age controls of the eight profiles. The dark and light grey shading represent the ranges of marine isotope stages; the ages of boundaries MIS 1-2, MIS 2-3, MIS 3-4, MIS 4-5 and MIS 5-6 are 10.2, 29.8, 61.0, 76.4 and 126.8 ka, respectively. GJP – Guojiapan; BGY – Beiguoyuan; XF – Xifeng; LT – Lingtai; YC – Yanchang; LC – Luochuan; TC – Tongchuan; BL – Bailu.

Harrison (2003) are usually at a similar level (sometimes the averages of MIS 2 are even higher) but, for this study, the AFs of MIS 2 are usually slightly lower than those of MIS 4. This difference is likely caused by the different age models (Lu & Sun, 2000; Kohfeld & Harrison, 2003; Kang *et al.* 2011, 2013). For the MS age model and independent chronologies (i.e.  $^{14}\text{C}$  and OSL dates), the mean AF of MIS 2 is lower than that of MIS 4; for the pedostratigraphy age model, the average of MIS 2 is higher than that of MIS 4 (Kohfeld & Harrison, 2003). In their compiled dataset, the profiles with only pedostratigraphy account for half of the total; this will greatly influence the evaluation and hence generate this difference. The ratio of MIS 2 to MIS 5, used to evaluate the contrast between glacial and interglacial (Kohfeld & Harrison, 2003), has a range from 1.79 to 4.23. This ratio varies from 0.8 to 22.6 and

has an average value of 5, according to the result of Kohfeld & Harrison (2003). The ratio summarized by Kohfeld & Harrison (2003) has a wider range than the result of this study. The difference is primarily due to landforms and dating methods of profiles, which make the values more variable (Lu & Sun, 2000; Nilson & Lehmkuhl, 2001).

The temporal pattern of AFs revealed by this study is similar to these records (Kohfeld & Harrison, 2003; Sun & An, 2005; Kang *et al.* 2015). On orbital timescales, the changes of ice volume in the Northern Hemisphere has been assumed to be the major drive of EAWM variations (Ding *et al.* 1995; Liu & Ding, 1998; Porter, 2001); moreover, the ice volume is primarily controlled by the Northern Hemisphere summer insolation at  $65^\circ\text{N}$ . The link between variations in high-latitude ice volume and the EAWM

**Table 1.** Average values of magnetic susceptibility (MS,  $10^{-8} \text{ m}^3 \text{ kg}^{-1}$ ), mean grain size (MGS,  $\mu\text{m}$ ) and aeolian flux (AF,  $\text{g cm}^{-2} \text{ ka}^{-1}$ ) during marine isotope stages (MIS) 1–5. NA – not available

	MIS 1			MIS 2			MIS 3			MIS 4			MIS 5			MIS 2/5		
	MS	MGS	AF	MS	MGS	AF	MS	MGS	AF	MS	MGS	AF	MS	MGS	AF	MS	MGS	AF
Guojiapan	95.6	34.73	33.46	35.6	45.92	75.89	38.6	31.96	50.76	36.2	38.48	69.26	72.0	25.36	19.44	0.50	1.81	3.90
Beiguoyuan	101.6	29.20	27.83	38.8	37.81	42.24	43.5	28.39	35.32	34.4	31.97	51.62	86.8	22.97	11.74	0.45	1.65	3.60
Xifeng	112.5	22.35	20.37	51.0	25.17	23.30	72.0	20.72	21.97	43.4	22.89	28.48	150.0	19.28	9.90	0.34	1.31	2.35
Lingtai	232.9	20.19	17.92	116.8	22.05	35.13	124.0	20.64	13.79	93.3	21.50	24.06	182.5	19.51	10.04	0.64	1.13	3.50
Yanchang	NA	NA	NA	37.6	35.83	16.91	69.2	26.27	24.68	41.5	29.29	41.89	163.7	22.22	9.43	0.23	1.61	1.79
Luochuan	217.4	18.79	18.01	90.9	22.05	13.48	140.5	18.62	15.92	82.4	18.56	21.34	250.6	16.28	5.75	0.36	1.35	2.34
Tongchuan	144.9	21.87	31.24	58.8	25.59	19.23	106.1	19.93	17.63	60.9	21.85	14.09	206.5	18.36	4.54	0.28	1.39	4.23
Bailu	212.5	16.02	11.94	146.7	17.09	11.15	204.4	14.35	9.86	180.1	14.64	13.81	244.6	13.46	3.62	0.60	1.27	3.08
<b>Statistics</b>																		
Median	144.9	21.87	20.37	54.9	25.38	21.26	89.0	20.68	19.80	52.2	22.37	26.27	173.1	19.39	9.67	0.41	1.37	3.29
Mean	159.6	23.31	22.97	72.0	28.94	29.67	99.8	22.61	23.74	71.5	24.90	33.07	169.6	19.68	9.31	0.42	1.44	3.10
Standard deviation	59.7	6.47	7.96	41.7	9.82	21.52	55.9	5.77	13.41	49.0	7.78	19.65	66.0	3.81	5.03	0.15	0.23	0.86
Maximum	232.9	34.73	33.46	146.7	45.92	75.89	204.4	31.96	50.76	180.1	38.48	69.26	250.6	25.36	19.44	0.64	1.81	4.23
Minimum	95.6	16.02	11.94	35.6	17.09	11.15	38.6	14.35	9.86	34.4	14.64	13.81	72.0	13.46	3.62	0.23	1.13	1.79

has been investigated intensively for a long time. In general, the mechanisms by which the ice volume drives the EAWM were discussed from the view of kinetics and thermodynamics (Ding *et al.* 1995). In detail, the extended ice sheets will reduce the vegetation cover and hence increase the albedo of the continental surface. As a result, the air in the Siberian region will be cooled and the Siberian High, the dominant atmospheric circulation system in the lower troposphere which controls almost the whole of continental Asia, will be enhanced. Secondly, the ice sheets can create a southwards movement of cold air. This dynamically affects atmospheric activity centres that cool the air in the middle latitudes and hence intensify the Siberian High. When the EAWM is strong, it carries more and coarser dust to the CLP, resulting in the increase of the AF and MGS in loess records (An *et al.* 1991a). Finally, the synchronous change of ice volume in the Northern Hemisphere and the effect of strong local convection in emission source results in high-amplitude fluctuations in AF on glacial–interglacial scales.

Moreover, the AF is also determined by the proportions of the dry/wet deposition processes of dust source regions, such as the coarser particles being more likely to be deposited through the dry deposition process over the CLP (Shi & Liu, 2011). Both dry and wet deposition processes contribute to the dust flux on the CLP according to modern observations (Yan *et al.* 2017). Dry and wet deposition processes are mainly controlled by extreme wind speed and precipitation, respectively. It is generally assumed that the dry deposition mostly happens during winter and spring, and the wet deposition mainly occurs during summer. Because the EAWM is much stronger in winter and spring, the precipitation is concentrated in summer. However, it is difficult to distinguish and quantify the contribution of dry and wet deposition from loess. In theory, the dry/wet deposition ratio depends on the climate background. The dry/wet deposition ratios are higher during glacial periods than during interglacial periods. During interglacial periods, the higher precipitation contributes to more wet deposition and hence increases the interglacial dust flux; as a result, it will reduce the contrast between glacial and interglacial AF records.

#### 4.b. Spatial gradients of the AF variation controlled by monsoon intensity

Although the spatial resolution is not very high, spatial patterns can be observed; a distinct increasing trend of AF values from south to north is observed, and the AF and  $\text{AF}_{\text{PM10}}$  are highest in the NW CLP (e.g. Guojiapan; Fig. 6). It should be noted that the AFs of Lingtai are higher than that of Xifeng, despite Lingtai being located to the south of Xifeng during MIS 2 and MIS 5. This NW–SE spatial gradient of AFs has also been reported elsewhere (Lu & Sun, 2000; Kohfeld & Harrison, 2003), and is affected by the integrated factors of source location and wind direction. The contrasting results at Lingtai might be the result of its particular geographical settings (Nilson & Lehmkuhl, 2001; Kohfeld & Harrison, 2003); close to the Qinling Mountains, the winds transferring the dust materials are suddenly reduced in speed as a result of their blocking effect. Greater volumes of dust accumulated in front of the Qinling Mountains because the reduced winds could carry the redundant dust materials, resulting in increasing local values of AF.

The spatial gradients in AF (the magnitude of differences of the values between one location and another location) during the last glacial are also greater than that of the last interglacial (Fig. 6a, b), with the exception of MIS 2 of the right transect in this study. This feature of AF is similar to that of MGS. The spatial gradient of MGS records over glacial–stadial timescales (i.e. MIS 2 and MIS 4) are greater (Fig. 6e, f), while the feature of MS is opposite. This implies that the EAWM plays an important part in AF fluctuations of the CLP. Numerous studies have suggested a warm and/or humid climate during MIS 5, with stronger (weaker) summer (winter) monsoon than during MIS 4 (e.g. An *et al.* 2014). Strengthening of the EASM circulation can lead to enhanced pedogenesis, while a weakened EAWM can decrease the competence and capacity of dust-bearing winds (Xiao *et al.* 1995). As a result, the information regarding pedogenesis and winds is preserved in the loess–palaeosol and can be extracted by the proxies, MS and

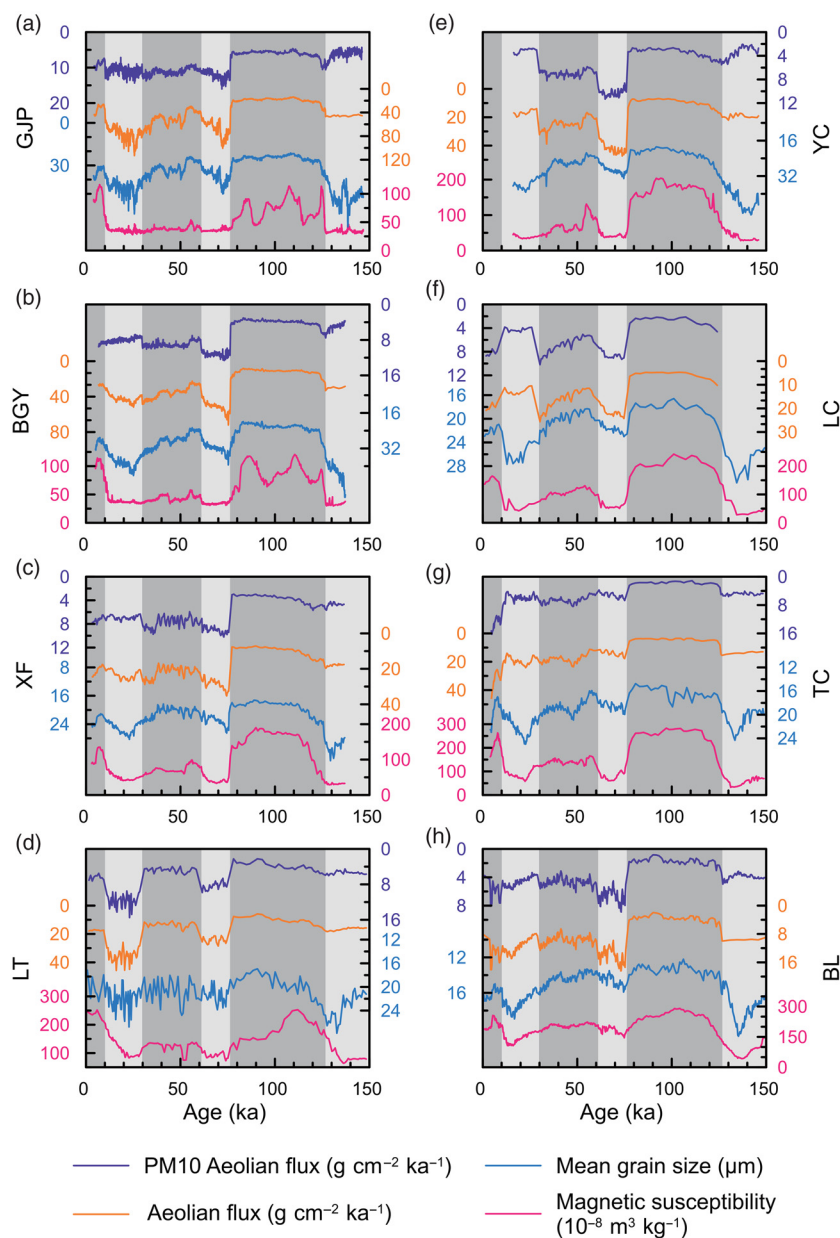


**Fig. 4.** The aeolian flux, PM10 aeolian flux, mean grain size and magnetic susceptibility during the last 150 ka. Shading and abbreviations as for Figure 3.

MGS (An *et al.* 2014). MS and MGS are the robust proxies of EASM and EAWM, respectively (An *et al.* 1990, 1991a,b). The spatial gradients of MS and MGS can be considered to be the spatial gradients of EASM and EAWM, respectively. The spatial gradients of MS and MGS records indicate that the EAWM has greater gradients in glacial periods, whereas the EASM has greater gradients in interglacial periods. The stronger spatial gradients of EAWM lead to greater gradients of MGS and AF, since they are both under the control of EAWM.

The grain-size distributions of modern dust and Chinese typical loess can be divided into three components, namely: ultrafine (< 2 μm), related to pedogenic processes; fine silt (2–10 μm), transported via long-term suspension processes; and medium silt, which is mainly transported via short-term suspension processes by near-surface winds (i.e. EAWM) (Pye & Zhou, 1989; Pye, 1995; Rea & Hovan, 1995; Sun *et al.* 2002, 2011; Vandenberghe, 2013). The samples at the NW CLP (proximal) have more medium silt material and less fine silt material, and the medium (fine) silt

component proportion is lower (higher) at the SE CLP (distal) (Sun *et al.* 2002; Vandenberghe, 2013). This spatial gradient will make the interpolation of AF more complicated, especially in the SE CLP. For example, the spatial gradients of AF (Fig. 6b) and MGS (Fig. 6f) at the east transect are lower than those at the west transect. This suggests that the signal of EAWM is weaker in the east transect, and the westerly jet becomes more important to variations in AF.

**4.c. Comparison between CLP and global dust records**

The prominent glacial–interglacial contrasts in AF records have also been detected from Biwa Lake (Xiao *et al.* 1997), Greenland (Ruth *et al.* 2007), Antarctica (EPICA Community Members, 2004; Lambert *et al.* 2012) and the Pacific Ocean (Hovan *et al.* 1991; Winckler *et al.* 2008; Jacobel *et al.* 2017) (Fig. 7). The AF values are generally higher during MIS 2, 4 and 6 than during MIS 1, 3 and 5, although the local boundary conditions of these



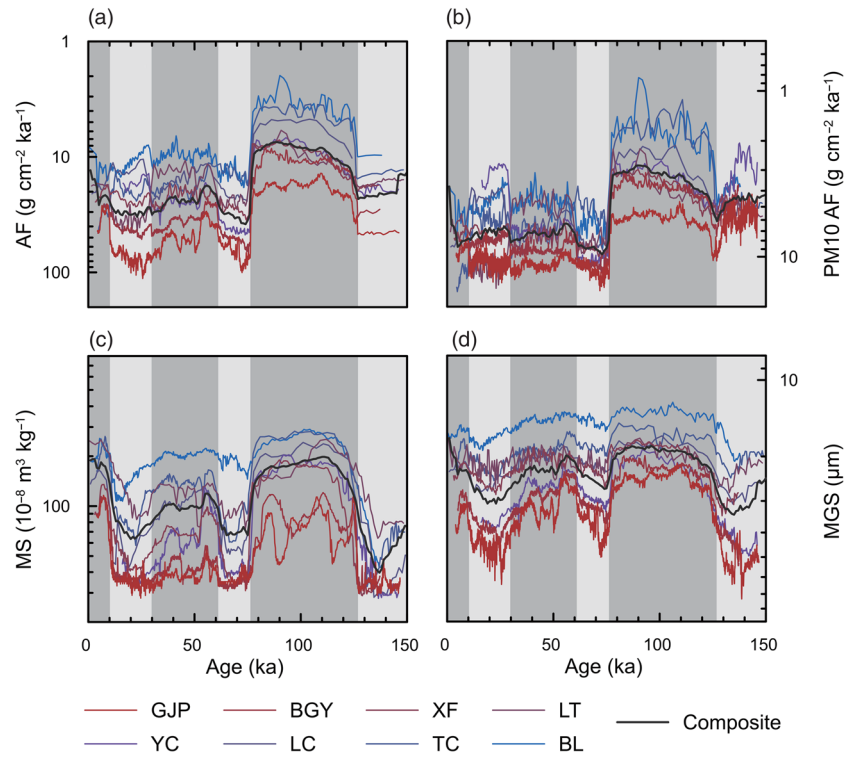


**Fig. 5.** (a) Aeolian flux (AF); (b) PM10 AF; (c) magnetic susceptibility (MS); and (d) mean grain size (MGS) for the eight profiles. Shading and abbreviations as for Figure 3.

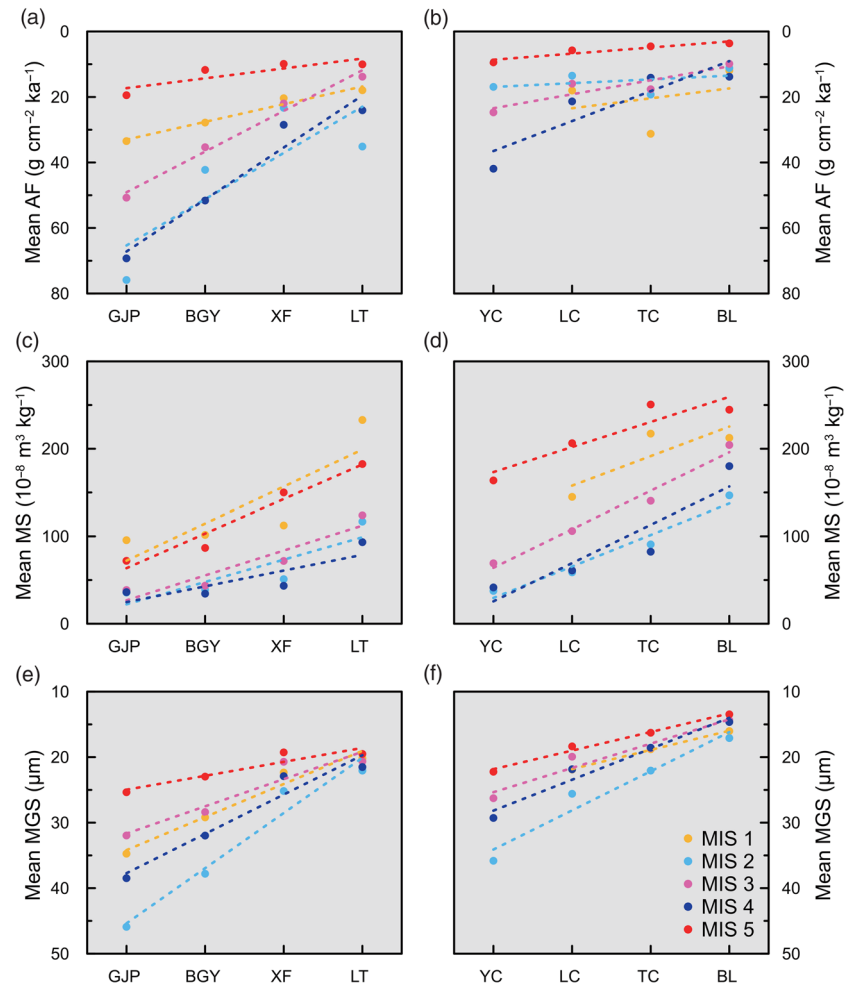


**Fig. 6.** Average (dots) and spatial gradients (lines) of aeolian flux (AF), magnetic susceptibility (MS) and mean grain size (MGS) during marine isotope stages (MIS) 1-5.



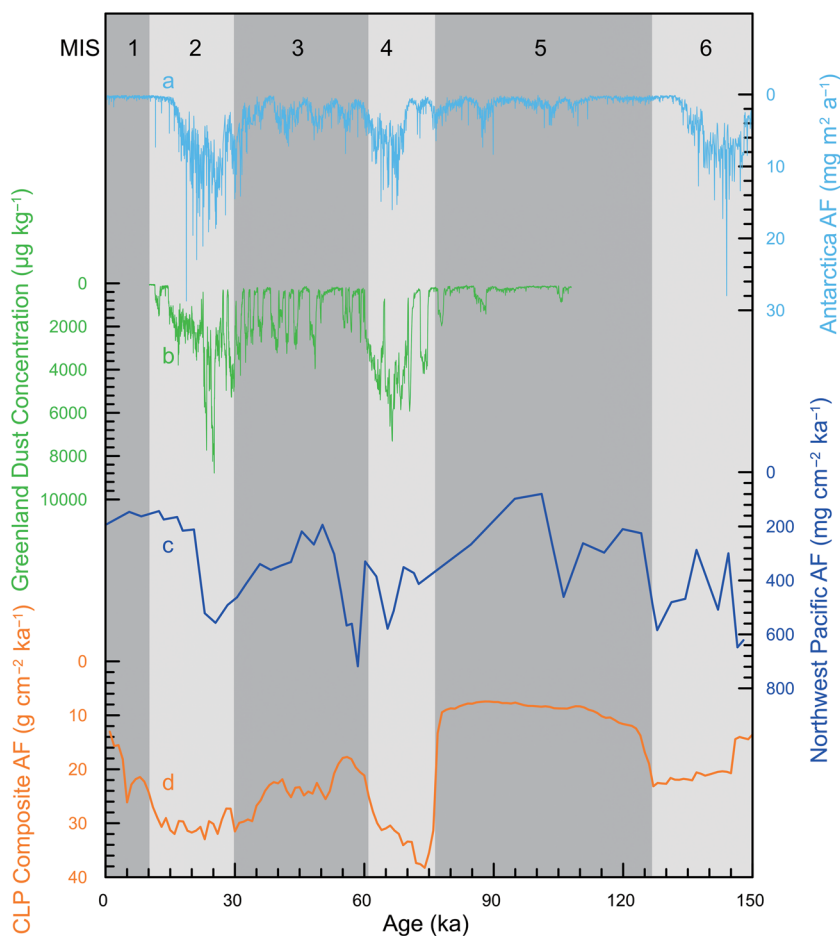


**Fig. 7.** Comparison of dust records from (a) Antarctica (light blue curve; Lambert *et al.* 2012); (b) Greenland (green curve; Ruth *et al.* 2007); (c) Northwest Pacific (dark blue curve; Hovan *et al.* 1991); and (d) CLP (orange curve; this study). Shading as for Figure 3.

regions vary hugely (Fig. 7d). In addition, these AF records are highly correlated with global ice volume. This implies that dust activities exhibited a global and universal response to climate change over late Pleistocene glacial cycles on orbital timescales (Winckler *et al.* 2008). The high-resolution AF records of Antarctica (Fig. 7a) and Greenland (Fig. 7b) show that there are some synchronous millennial variations. These records suggest that the millennial component of global climate changes have an influence on AF. However, there are also some local signals preserved in these records. For example, during interglacial and/or interstadial periods, the dust deposition rate is very close to zero both in Antarctica (Fig. 7a) and Greenland (Fig. 7b). This indicates that the deposition process temporarily stopped during these periods. In contrast, the AF values in the CLP (Fig. 7d) were still high during interglacial and/or interstadial periods (An *et al.* 1991a; Sun & An, 2002, 2005). This suggests that the dust activities remained on a certain scale as a result of a sufficient dust supply and favourable transmission (Shi & Liu, 2011; An *et al.* 2014; Liu *et al.* 2017), even when the global climate was very warm; the long-distance dust transmission might have been interrupted for remote sinks, however.

### 5. Conclusions

In this study, we employed a uniform age model based on OSL chronologies to reconstruct the AFs of eight profiles on the CLP since the last interglacial. The results indicate that there are clear temporal and spatial patterns in the CLP; in addition, the patterns

are compatible with the records of MS and GS. The AF and  $\text{AF}_{\text{PM}_{10}}$  records are higher and more variable in glacial than in interglacial periods, and are influenced by the synchronous change of ice volume in the Northern Hemisphere and the effect of strong local convection in emission sources. The MGS, AF and  $\text{AF}_{\text{PM}_{10}}$  values of SE profiles are generally lower than that of NW profiles, while MS records show an opposite trend. This study has allowed great improvements to the reconstruction of AFs as a result of our uniform age model and reliable bulk density data. More importantly, this age model can be used to refine the other AF datasets (e.g. DIRTMAP dataset; Kohfeld & Harrison 2001) and hence improve the spatial resolution. Furthermore, this work is expected to provide key parameters for the model, allowing the assessment of dust-climate interactions.

**Acknowledgements.** This work was supported by the National Key Research and Development Program of China (2016YFA0601902) and the National Natural Science Foundation of China (41525008 and 41472163).

**Declaration of interest.** None.

### References

An Z, Wu G, Li J, Sun Y, Liu Y, Zhou W, Cai Y, Duan A, Li L, Mao J, Cheng H, Shi Z, Tan L, Yan H, Ao H, Chang H and Feng J (2015) Global monsoon dynamics and climate change. *Annual Review of Earth and Planetary Sciences* 43, 29–77.  
 An Z, Kukla G, Porter SC and Xiao J (1991a) Late quaternary dust flow on the Chinese Loess Plateau. *Catena* 18, 125–32.

- An Z, Kukla GJ, Porter SC and Xiao J (1991b) Magnetic susceptibility evidence of monsoon variation on the Loess Plateau of central China during the last 130,000 years. *Quaternary Research* **36**, 29–36.
- An Z, Kutzbach JE, Prell WL and Porter SC (2001) Evolution of Asian monsoons and phased uplift of the Himalaya-Tibetan plateau since Late Miocene times. *Nature* **411**, 62–6.
- An Z, Liu T, Lu Y, Porter SC, Kukla G, Wu X and Hua Y (1990) The long-term paleomonsoon variation recorded by the loess-paleosol sequence in central China. *Quaternary International* **7–8**, 91–5.
- An Z, Sun Y, Zhou W, Liu W, Qiang X, Wang X, Xian F, Cheng P and Burr GS (2014) Chinese loess and the East Asian monsoon. In *Late Cenozoic Climate Change in Asia* (ed. Z An), pp. 23–143. Dordrecht: Springer Netherlands.
- Berger A (1978) Long-term variations of daily insolation and Quaternary climatic changes. *Journal of the Atmospheric Sciences* **35**, 2362–67.
- Cheng H, Edwards RL, Sinha A, Spötl C, Yi L, Chen S, Kelly M, Kathayat G, Wang X, Li X, Kong X, Wang Y, Ning Y and Zhang H (2016) The Asian monsoon over the past 640,000 years and ice age terminations. *Nature* **534**, 640–46.
- Derbyshire E (2003) Loess, and the dust indicators and records of terrestrial and marine palaeoenvironments (DIRTMAP) database. *Quaternary Science Reviews* **22**, 1813–9.
- Ding Z, Liu T, Rutter N, Yu Z, Guo Z and Zhu R (1995) Ice-volume forcing of East Asian winter monsoon variations in the past 800,000 years. *Quaternary Research* **44**, 149–59.
- Ding ZL, Derbyshire E, Yang SL, Yu ZW, Xiong SF and Liu TS (2002) Stacked 2.6-Ma grain size record from the Chinese loess based on five sections and correlation with the deep-sea  $\delta^{18}\text{O}$  record. *Paleoceanography* **17**, 5-1–5-21.
- Dong Y, Wu N, Li F, Huang L and Wen W (2015) Time-transgressive nature of the magnetic susceptibility record across the Chinese Loess Plateau at the Pleistocene/Holocene transition (ed. C. Li). *PLOS ONE* **10**, e0133541.
- Engelbrecht JP and Derbyshire E (2010) Airborne mineral dust. *Elements* **6**, 241–6.
- EPICA Community Members (2004) Eight glacial cycles from an Antarctic ice core. *Nature* **429**, 623–8.
- Guo Z, Liu T, Guiot J, Wu N, Lü H, Han J, Liu J and Gu Z (1996) High frequency pulses of East Asian monsoon climate in the last two glaciations: link with the North Atlantic. *Climate Dynamics* **12**, 701–9.
- Guo ZT, Ruddiman WF, Hao QZ, Wu HB, Qiao YS, Zhu RX, Peng SZ, Wei JJ, Yuan BY and Liu TS (2002) Onset of Asian desertification by 22 Myr ago inferred from loess deposits in China. *Nature* **416**, 159–63.
- Harrison SP, Kohfeld KE, Roelandt C and Claquin T (2001) The role of dust in climate changes today, at the last glacial maximum and in the future. *Earth-Science Reviews* **54**, 43–80.
- Hovan SA, Rea DK and Pisias NG (1991) Late Pleistocene continental climate and oceanic variability recorded in northwest Pacific sediments. *Paleoceanography* **6**, 349–70.
- Jacobel AW, McManus JF, Anderson RF and Winckler G (2017) Climate-related response of dust flux to the central equatorial Pacific over the past 150 kyr. *Earth and Planetary Science Letters* **457**, 160–72.
- Kang S, Lu Y and Wang X (2011) Closely-spaced recuperated OSL dating of the last interglacial paleosol in the southeastern margin of the Chinese Loess Plateau. *Quaternary Geochronology* **6**, 480–90.
- Kang S, Roberts HM, Wang X, An Z and Wang M (2015) Mass accumulation rate changes in Chinese loess during MIS 2, and asynchrony with records from Greenland ice cores and North Pacific Ocean sediments during the Last Glacial Maximum. *Aeolian Research* **19**, 251–8.
- Kang S, Wang X and Lu Y (2013) Quartz OSL chronology and dust accumulation rate changes since the Last Glacial at Weinan on the southeastern Chinese Loess Plateau. *Boreas* **42**, 815–29.
- Kohfeld K and Harrison SP (2003) Glacial-interglacial changes in dust deposition on the Chinese Loess Plateau. *Quaternary Science Reviews* **22**, 1859–78.
- Kohfeld KE and Harrison SP (2001) DIRTMAP: the geological record of dust. *Earth-Science Reviews* **54**, 81–114.
- Kukla G (1987) Loess stratigraphy in central China. *Quaternary Science Reviews* **6**, 191–219.
- Kukla G and An Z (1989) Loess stratigraphy in central China. *Palaeogeography, Palaeoclimatology, Palaeoecology* **72**, 203–25.
- Lai Z, Wintle AG and Thomas DSG (2007) Rates of dust deposition between 50 ka and 20 ka revealed by OSL dating at Yuanbao on the Chinese Loess Plateau. *Palaeogeography, Palaeoclimatology, Palaeoecology* **248**, 431–9.
- Lai Z-P and Wintle AG (2006) Locating the boundary between the Pleistocene and the Holocene in Chinese loess using luminescence. *The Holocene* **16**, 893–9.
- Lambert F, Bigler M, Steffensen JP, Hutterli M and Fischer H (2012) Centennial mineral dust variability in high-resolution ice core data from Dome C, Antarctica. *Climate of the Past* **8**, 609–23.
- Lisiecki LE and Raymo ME (2005) A Pliocene-Pleistocene stack of 57 globally distributed benthic  $\delta^{18}\text{O}$  records. *Paleoceanography* **20**, PA1003, doi: [10.1029/2004PA001071](https://doi.org/10.1029/2004PA001071).
- Liu T (1985) *Loess and the Environment*. Beijing, China: China Ocean Press, 251 pp.
- Liu T and Ding Z (1998) Chinese loess and the paleomonsoon. *Annual Review of Earth and Planetary Sciences* **26**, 111–45.
- Liu X-J, Xiao G, Chongyi E, Li X, Lai Z, Yu L and Wang Z (2017) Accumulation and erosion of aeolian sediments in the northeastern Qinghai-Tibetan Plateau and implications for provenance to the Chinese Loess Plateau. *Journal of Asian Earth Sciences* **135**, 166–74.
- Lu H and An Z (1997) The influence of pre-treatment to grainsize analysis results of loess. *Chinese Science Bulletin* **42**, 2535–8.
- Lu H, Stevens T, Yi S and Sun X (2006) An erosional hiatus in Chinese loess sequences revealed by closely spaced optical dating. *Chinese Science Bulletin* **51**, 2253–9.
- Lu H and Sun D (2000) Pathways of dust input to the Chinese Loess Plateau during the last glacial and interglacial periods. *Catena* **40**, 251–61.
- Lu YC, Wang XL and Wintle AG (2007) A new OSL chronology for dust accumulation in the last 130,000 yr for the Chinese Loess Plateau. *Quaternary Research* **67**, 152–60.
- Ma L, Li Y, Liu X and Sun Y (2017) Registration of precession signal in the Last Interglacial paleosol ( $S_1$ ) on the Chinese Loess Plateau. *Geochemistry, Geophysics, Geosystems* **18**, 3964–75.
- Maher BA, Prospero JM, Mackie D, Gaiero D, Hesse PP and Balkanski Y (2010) Global connections between aeolian dust, climate and ocean biogeochemistry at the present day and at the last glacial maximum. *Earth-Science Reviews* **99**, 61–97.
- Muhs DR (2013) The geologic records of dust in the Quaternary. *Aeolian Research* **9**, 3–48.
- Nilson E and Lehmkuhl F (2001) Interpreting temporal patterns in the late Quaternary dust flux from Asia to the North Pacific. *Quaternary International*, **76–77**, 67–76.
- Peng Y, Xiao J, Nakamura T, Liu B and Inouchi Y (2005) Holocene East Asian monsoonal precipitation pattern revealed by grain-size distribution of core sediments of Daihai Lake in Inner Mongolia of north-central China. *Earth and Planetary Science Letters* **233**, 467–79.
- Porter SC (2001) Chinese loess record of monsoon climate during the last glacial-interglacial cycle. *Earth-Science Reviews* **54**, 115–28.
- Porter SC and An Z (1995) Correlation between climate events in the North Atlantic and China during last glaciation. *Nature* **375**, 305–8.
- Prospero JM (2002) Environmental characterization of global sources of atmospheric soil dust identified with the NIMBUS 7 Total Ozone Mapping Spectrometer (TOMS) absorbing aerosol product. *Reviews of Geophysics* **40**, 2-1–2-31.
- Pye K (1995) The nature, origin and accumulation of loess. *Aeolian Sediments in the Quaternary Record* **14**, 653–67.
- Pye K and Krinsley DH (1986) Diagenetic carbonate and evaporite minerals in Rotliegend aeolian sandstones of the southern North Sea: their nature and relationship to secondary porosity development. *Clay Minerals* **21**, 443–57.
- Pye K and Zhou L-P (1989) Late Pleistocene and Holocene aeolian dust deposition in north China and the northwest Pacific Ocean. *Palaeogeography, Palaeoclimatology, Palaeoecology* **73**, 11–23.
- Qiang X, An Z, Song Y, Chang H, Sun Y, Liu W, Ao H, Dong J, Fu C, Wu F, Lu F, Cai Y, Zhou W, Cao J, Xu X and Ai L (2011) New eolian red clay sequence on the western Chinese Loess Plateau linked to onset of Asian desertification about 25 Ma ago. *Science China Earth Sciences* **54**, 136–44.

- Rao Z, Chen F, Cheng H, Liu W, Wang G, Lai Z and Bloemendal J (2013) High-resolution summer precipitation variations in the western Chinese Loess Plateau during the last glacial. *Scientific Reports* **3**, article no. 2785(2013).
- Rea DK (1994) The paleoclimatic record provided by eolian deposition in the deep sea: the geologic history of wind. *Reviews of Geophysics* **32**, 159.
- Rea DK and Hovan SA (1995) Grain size distribution and depositional processes of the mineral component of abyssal sediments: lessons from the North Pacific. *Paleoceanography* **10**, 251–8.
- Rea DK, Snoeckx H and Joseph LH (1998) Late Cenozoic eolian deposition in the North Pacific: Asian drying, Tibetan uplift, and cooling of the northern hemisphere. *Paleoceanography* **13**, 215–24.
- Ruth U, Bigler M, Röthlisberger R, Siggaard-Andersen M-L, Kipfstuhl S, Goto-Azuma K, Hansson ME, Johnsen SJ, Lu H and Steffensen JP (2007) Ice core evidence for a very tight link between North Atlantic and east Asian glacial climate. *Geophysical Research Letters* **34**, L03706.
- Shao Y, Wyrwoll K-H, Chappell A, Huang J, Lin Z, McTainsh GH, Mikami M, Tanaka TY, Wang X and Yoon S (2011) Dust cycle: an emerging core theme in Earth system science. *Aeolian Research* **2**, 181–204.
- Shi Z and Liu X (2011) Distinguishing the provenance of fine-grained eolian dust over the Chinese Loess Plateau from a modelling perspective. *Tellus B: Chemical and Physical Meteorology* **63**, 959–70.
- Stevens T, Armitage SJ, Lu H and Thomas DSG (2006) Sedimentation and diagenesis of Chinese loess: implications for the preservation of continuous, high-resolution climate records. *Geology* **34**, 849.
- Stevens T, Buyllaert J-P, Thiel C, Újvári G, Yi S, Murray AS, Frechen M and Lu H (2018) Ice-volume-forced erosion of the Chinese Loess Plateau global Quaternary stratotype site. *Nature Communications* **9**, 983.
- Stevens T, Lu H, Thomas DSG and Armitage SJ (2008) Optical dating of abrupt shifts in the late Pleistocene East Asian monsoon. *Geology* **36**, 415.
- Stevens T, Thomas D, Armitage S, Lunn H and Lu H (2007) Reinterpreting climate proxy records from late Quaternary Chinese loess: a detailed OSL investigation. *Earth-Science Reviews* **80**, 111–36.
- Sun D, Bloemendal J, Rea DK, Vandenberghe J, Jiang F, An Z and Su R (2002) Grain-size distribution function of polymodal sediments in hydraulic and aeolian environments, and numerical partitioning of the sedimentary components. *Sedimentary Geology* **152**, 263–77.
- Sun D, Su R, Li Z and Lu H (2011) The ultrafine component in Chinese loess and its variation over the past 7.6 Ma: implications for the history of pedogenesis. *Sedimentology* **58**, 916–35.
- Sun Y and An Z (2002) History and variability of Asian interior aridity recorded by eolian flux in the Chinese Loess Plateau during the past 7 Ma. *Science in China Series D* **45**, 420.
- Sun Y and An Z (2005) Late Pliocene-Pleistocene changes in mass accumulation rates of eolian deposits on the central Chinese Loess Plateau. *Journal of Geophysical Research* **110**.
- Sun Y, An Z, Zhou J and Lu X (2000) Dry bulk density of loess samples measured by the oil-soaked method. *Geological Review* **46**, 220–4.
- Sun Y, Clemens SC, An Z and Yu Z (2006a) Astronomical timescale and palaeoclimatic implication of stacked 3.6-Myr monsoon records from the Chinese Loess Plateau. *Quaternary Science Reviews* **25**, 33–48.
- Sun Y, Clemens SC, Morrill C, Lin X, Wang X and An Z (2012) Influence of Atlantic meridional overturning circulation on the East Asian winter monsoon. *Nature Geoscience* **5**, 46–9.
- Sun Y, Lu H and An Z (2006b) Grain size of loess, palaeosol and Red Clay deposits on the Chinese Loess Plateau: significance for understanding pedogenic alteration and palaeomonsoon evolution. *Palaeogeography, Palaeoclimatology, Palaeoecology* **241**, 129–38.
- Sun Y, Wang X, Liu Q and Clemens SC (2010) Impacts of post-depositional processes on rapid monsoon signals recorded by the last glacial loess deposits of northern China. *Earth and Planetary Science Letters* **289**, 171–9.
- Sun Y, Yin Q, Crucifix M, Clemens SC, Araya-Melo P, Liu W, Qiang X, Liu Q, Zhao H, Liang L, Chen H, Li Y, Zhang L, Dong G, Li M, Zhou W, Berger A and An Z (2019) Diverse manifestations of the mid-Pleistocene climate transition. *Nature Communications* **10**, 352.
- Vandenberghe J (2013) Grain size of fine-grained windblown sediment: a powerful proxy for process identification. *Earth-Science Reviews* **121**, 18–30.
- Winckler G, Anderson RF, Fleisher MQ, McGee D and Mahowald N (2008) Covariant glacial-interglacial dust fluxes in the equatorial Pacific and Antarctica. *Science* **320**, 93–6.
- Wu J, Lu H, Yi S, Xu Z, Gu Y, Liang C, Cui M and Sun X (2019) Establishing a high-resolution luminescence chronology for the Zhenbeitai sand-loess section at Yulin, North-Central China. *Quaternary Geochronology* **49**, 78–84.
- Xiao J, Inouchi Y, Kumai H, Yoshikawa S, Kondo Y, Liu T and An Z (1997) Eolian quartz flux to Lake Biwa, central Japan, over the past 145,000 years. *Quaternary Research* **48**, 48–57.
- Xiao J, Porter SC, An Z, Kumai H and Yoshikawa S (1995) Grain size of quartz as an indicator of winter monsoon strength on the Loess Plateau of central China during the last 130,000 yr. *Quaternary Research* **43**, 22–9.
- Xu Z, Stevens T, Yi S, Mason JA and Lu H (2018) Seesaw pattern in dust accumulation on the Chinese Loess Plateau forced by late glacial shifts in the East Asian monsoon. *Geology* **46**, 871–4.
- Yan Y, Chen H, Liang L, Ma L, Liu X, Liu H and Sun Y (2017) Meteorological constraints on characteristics of daily dustfall in Xi'an. *Atmospheric Environment* **158**, 98–104.
- Yung YL, Lee T, Wang C-H and Shieh Y-T (1996) Dust: a diagnostic of the hydrologic cycle during the Last Glacial Maximum. *Science* **271**, 962–3.
- Zachos J, Pagani M, Sloan L, Thomas E & Billups K (2001) Trends, rhythms, and aberrations in global climate 65 Ma to present. *Science* **292**, 686–93.
- Zhang J, Li S-H, Sun J and Hao Q (2018a) Fake age hiatus in a loess section revealed by OSL dating of calcrete nodules. *Journal of Asian Earth Sciences* **155**, 139–45.
- Zhang W, Chen J, Ji J and Li G (2016) Evolving flux of Asian dust in the North Pacific Ocean since the late Oligocene. *Aeolian Research* **23**, 11–20.
- Zhang W, De Vleeschouwer D, Shen J, Zhang Z and Zeng L (2018b) Orbital time scale records of Asian eolian dust from the Sea of Japan since the early Pliocene. *Quaternary Science Reviews* **187**, 157–67.